Journal of Drug Delivery Science and Technology 45 (2018) 28–38

Contents lists available at ScienceDirect

Journal of Drug Delivery Science and Technology

journal homepage: www.elsevier.com/locate/jddst

Lyophilization model of mannitol water solution in a laboratory scale lyophilizer

J. Ravnik[a], I. Golobič[b], A. Sitar[b], M. Avanzo[c], Š. Irman[c], K. Kočevar[c], M. Cegnar[c], M. Zadravec[a], M. Ramšak[a], M. Hriberšek[a,*]

[a] Faculty of Mechanical Engineering, University of Maribor, Smetanova Ulica 17, SI-2000 Maribor, Slovenia
[b] Faculty of Mechanical Engineering, University of Ljubljana, Aškerčeva Cesta 6, SI-1000 Ljubljana, Slovenia
[c] LEK d.d., Verovškova 57, SI-1526 Ljubljana, Slovenia

ARTICLE INFO

Keywords:
Lyophilization
Freeze-drying
Vial
Heat and mass transfer
Finite difference model
Sublimation

ABSTRACT

The paper reports on the development of a numerical model for the simulation of a lyophilization process in a vial. Experimental analysis is presented of lyophilization dynamics inside a single vial in a laboratory scale lyophilizer. The problems of lyophilization modelling of a mannitol water solution are covered in detail. The effects of the small scale of the laboratory device with respect to a correct definition of boundary conditions for the numerical simulations are described, especially the effect of the comparatively high temperatures of the chamber walls. In the numerical model, a 1D vial approximation of the governing equations of heat and mass transport with moving front between the frozen and porous part of the cake is used and solved in a time stepping nonlinear iteration procedure. A water vapour diffusion model, implemented in the mass conservation equations, based on the Knudsen model of diffusivities, is applied and linked to the typical pore size of the porous cake. A front tracking scheme with moving computational grid is applied, and a dedicated sub-model of surface layer ice sublimation is introduced, based on the one-sided vapour diffusion model. The comparison of the numerical and the experimental results show that the developed numerical model is able to capture the transition points from primary to secondary drying very accurately, with accompanying accurate capturing of the temperature levels inside of the drying material.

1. Introduction

Development of lyophilization procedures for different formulations in the pharmaceutical industry typically requires extensive experimental testing on laboratory scale lyophilizers. Lyophilization can be divided into three stages. The first stage is freezing of the base compound to solidify it, then the surrounding pressure is lowered to a level where the frozen solvent (typically water) starts to sublimate. At this point, the second stage begins, represented by the sublimation process of the ice (primary drying). After the sublimation process ends, the third stage starts with desorption of the bounded water in the dried material (secondary drying). Because the freeze-drying process is performed at relatively low temperatures, the quality of formulations is preserved, and at the same time, their stability is increased [8]. In order to reduce the number of required test runs, modelling and computer simulations of the process in the framework of dedicated computational models can be of significant help. Among different modelling approaches, computational models, based on the theory of transport phenomena, offer several advantages over some simplified, rate-based approaches. Early works of [14] are among the simplest, but report on all basic problems of lyophilization modelling.

When a drying model is developed at a differential level using Partial Differential Equations (PDE) [9,11,15], the governing heat and mass transfer processes can be simulated in three-dimensional geometries of the drying media and with full time resolution of the process. However, when the lyophilization process is concerned, the pharmaceutical process is, typically, performed with the drying formulation placed inside a vial. In order to achieve high production quantities, several thousand vials are, typically, placed on several trays inside a vacuum drying chamber. This imposes severe requirements on the computational model, as a full 3D resolution of the drying and condensation chamber, coupled with a full 3D resolution of the interior of vials, yields extremely large numbers of system unknowns. Adding the necessity to perform the time stepping procedure during the entire lyophilization cycle, this leads to computationally non-feasible approaches. This can be overcome by constructing a lyophilization model

* Corresponding author.
E-mail address: matjaz.hribersek@um.si (M. Hriberšek).

https://doi.org/10.1016/j.jddst.2018.02.015
Received 29 November 2017; Received in revised form 5 February 2018; Accepted 22 February 2018
Available online 27 February 2018
1773-2247/

Nomenclature

$c_{p,1}$	effective specific heat $[J/kg]$ for a mixture of porous cake, water vapour and inert gas in region 1
$c_{p,g}$	specific heat $[J/kg]$ for a mixture of water vapour and inert gas in region 1
ρ_1	effective density $[kg/m^3]$ for a mixture of porous cake, water vapour and inert gas in region 1
ρ_2	effective density $[kg/m^3]$ of frozen cake in region 2
$\rho_{1,p}$	density $[kg/m^3]$ of porous cake in region 1
ΔH_v	enthalpy of vapourization, $[J/kg]$
ΔH_s	enthalpy of sublimation, $[J/kg]$
λ_1	thermal conductivity $[W/mK]$ for a mixture of porous cake, water vapour and inert gas in region 1
λ_2	thermal conductivity $[W/mK]$ of frozen cake in region 2
$\overrightarrow{N_v}$	mass flux $[kg/m^2s]$ of water vapour in region 1
$\overrightarrow{N_i}$	mass flux $[kg/m^2s]$ of inert gas in region 1
C	concentration of adsorbed water in region 1 $[kg/kg]$
$C^\star$	equilibrium concentration of adsorbed water in region 1 $[kg/kg]$
v_n	speed of movement of the sublimation front, $[m/s]$
$N_{v,n}$	mass flux $[kg/m^2s]$ of water vapour in region 1 a in direction normal to the sublimation front
k_g	water desorption rate $[s^{-1}]$
$\in$	porosity of mannitol cake in region 1, $[-]$
M_v	molecular weight of water, $[kg/kmol]$
M_i	molecular weight of inert gas, $[kg/kmol]$
R	ideal gas constant, $[8314\,J/kmolK]$
p_v	partial water vapour pressure in region 1, $[Pa]$
p_i	partial inert gas pressure in region 1, $[Pa]$
$p_v^\star$	equilibrium partial water vapour pressure at sublimation front $[Pa]$
T	temperature, $[K]$
t	time, $[s]$
C_{01}	model parameter for relative Darcy flow permeability
C_1	model parameter for relative Knudsen flow permeability, $[m]$
C_2	ratio of bulk diffusivity in porous medium to free gas bulk diffusivuty, $[-]$
$D_{v,i}$	diffusivity of a binary mixture of water vapour and inert gas in region 1
$\mathscr{D}_{v,i}$	diffusivity of a binary mixture of water vapour and inert gas in free space
K_v	Knudsen diffusivity for water vapour, $[m^2/s]$
K_i	Knudsen diffusivity for inert gas, $[m^2/s]$
K_{mx}	Knudsen diffusivity for a mixture of water vapour and inert gas, $[m^2/s]$
μ_{mx}	viscosity of mixture of water vapour and inert gas in region 1, $[kg/ms]$
k_1	k_3 bulk diffusivity constant
k_2	k_4 self diffusivity constant
d_p	pore diameter, $[m]$
τ	tortuosity, $[-]$
λ	molecular free path, $[m]$
$\overrightarrow{J}'$	J'_v molar flux $[mol/m^2s]$ of water vapour from surface ice layer
$\dot{m}_v$	water vapour mass flux
$\dot{Q}_{us}$	$\dot{Q}_{ls}$ heat flux from upper and lower shelf

that splits the computation of the problem into two basic steps: Computation of the heat and mass transfer problem of ice sublimation and desorption inside a vial, performed typically with some simplified model, which is then coupled to the general 3D flow field with heat and mass transfer computation in the rest of the lyophilization chamber. The main requirement on the computational model for lyophilization inside a vial is the ability to deliver good spatial and temporal resolution of the drying process by keeping a low single vial computational cost. In order to achieve this goal, the computational model has to be simplified carefully, generally leading to models with a lower degree of spatial resolution, but a higher degree of time stepping accuracy.

Numerical modelling of the lyophilization process is significantly different from other drying procedures because of the much lower system pressure, which almost eliminates the convection mechanism of heat transfer. Therefore, the conduction and the radiation play a major role in the heat transfer process [4,14,16]. Next, since the drying material is highly porous, it cannot be modelled directly due to an extremely complex internal structure. The composition of the internal structure depends heavily on the freezing stage. Therefore, the dry material had to be modelled using the porous model approach. The freeze-drying process, particularly the mass and momentum transfer of the solvent, take place at a very low static pressure, where the free-range between the molecules is very large and, consequently, also the Knudsen number, which questions the correctness of using the governing equations that are developed for the continuum. This could pose problems in modelling of the momentum transfer and condensation of the solvent (water) in the lyophilizer chamber and condenser [1,13]. However, when the drying chamber is concerned, the Knudsen number values are not critical and the use of continuum models is justifiable. Among several important scientific contributions, the ”sorption-sublimation” model described in Refs. [9,10,12,15,18], has proven to be accurate and successful in simulating the freeze-drying process in vial solution. [10]; solved the freeze-drying model using the Finite Element Method (FEM) with the Arbitrary Lagrangian-Eulerian (ALE) scheme. A 2D axisymmetrical model to the freeze-drying problem in a vial for protein Bovine Somatotropin (BST) and skim milk was developed, where the latter problem has been treated as a 1D problem. [16]; improved the boundary conditions of the model by including heat radiation, and solved the governing equations using the Finite Difference Method (FDM). The numerical model was used to study the freeze-drying of skim milk in vials, and three different cases were investigated. They changed the vial position (centre or corner) and set different process controls for not exceeding the melting and scorch temperatures.

In the work of [19]; the orthogonal collocations method was applied for solution of the mono-dimensional lyophilization model, and they also proposed two additional simplified models. Comparisons were made with experimental results, obtained for the centre of the shelf vial position. In the work of [2]; the effect of the batch nonuniformity was studied by means of a coupled CFD and mono-dimensional vial lyophilization model, with a clear outcome of faster drying rates for the edge vial positions.

In order to develop a dedicated lyophilization model for modelling of the heat and mass transfer processes inside a simplified vial geometry, that could be used in a Computational Fluid Dynamics (CFD) approach for modelling momentum, heat and mass transfer outside the vials, which, in turn, also interacts with vials, experimental data is necessary. As there is a limited possibility to interact with an industrial scale lyophilization process, the experiments are, typically, performed with vials in a laboratory scale lyophilizer. Data, that are needed to verify a lyophilization computational model, consist of temperature dynamics inside the vial, important for the determination of the transition point between the primary and the secondary drying stages, but also a temperature field in the surroundings of a vial. As heat conduction and heat radiation are the most important heat transfer mechanisms, temperatures of the shelf and drying chamber walls are needed in order to impose proper boundary conditions for the numerical model. There are also other phenomena that can influence the validity of the model significantly. These include the data on the extent of the contact

area between the vial bottom and the shelf, and also on the structural behaviour of the drying formulation. These data can be problem specific, therefore careful experimental planning is required.

The paper is organised as follows. Section 2 describes the freeze-drying in a vial in more detail, with special emphasis on modelling of the heat and mass transfer phenomena. Section 3 reports on the experimental procedures and methods, used in the determination of lyophilization kinetics inside a vial, and in determination of relevant boundary conditions on the vial walls. The derived governing equations (mathematical model), with their description, are reported in Section 4. Section 5 covers the description of the implemented numerical discretization of governing equations, yielding the complete numerical model for freeze-drying simulation in vials. Computational examples, with validation, results and discussion, are presented in Section 6. The paper ends with the conclusion in Section 7.

2. Freeze-drying in a vial

In the first drying stage, in the vial there coexist a frozen part of the cake (Region 2) in contact with a porous, ice free part of the cake (Region 1), Fig. 1. Both regions are connected by a sublimation front, where drying of the frozen solvent (water) takes place under sublimation conditions. As the ice is removed in the Region 1, the desorption process starts immediately, and coexists with the sublimation process until the end of the primary drying stage. After all of the ice is removed, the desorption process becomes the only mechanism of moisture removal, which is the main characteristic of the second drying stage. In this stage, the temperature of the shelves is increased, while still taking care that the product temperature does not exceed its glass transition temperature, so that a collapse does not occur.

The main driving force of sublimation is the pressure difference between the vapour pressure at the sublimation front and partial vapour pressure in the surroundings of the vial. In order to establish a sustainable drying process, heat must be supplied to the drying substance. As the total pressure in a sublimation dryer is, typically, around $10Pa$, the only significant heat transfer mechanisms are heat conduction from the lower shelf and heat radiation from the surrounding walls. As the vial bottom does not match perfectly the lower shelf shape, the heat from below is a combination of heat conduction at the vial contact area and heat radiation from the lower shelf to the vial bottom. Since there is another shelf above the vial, the heat from above enters the vial mainly via radiation, even though the product is partially shielded by the stopper. There exist also the effect of the heat radiation and convection to the side surface of the vial, which depend on the number and position

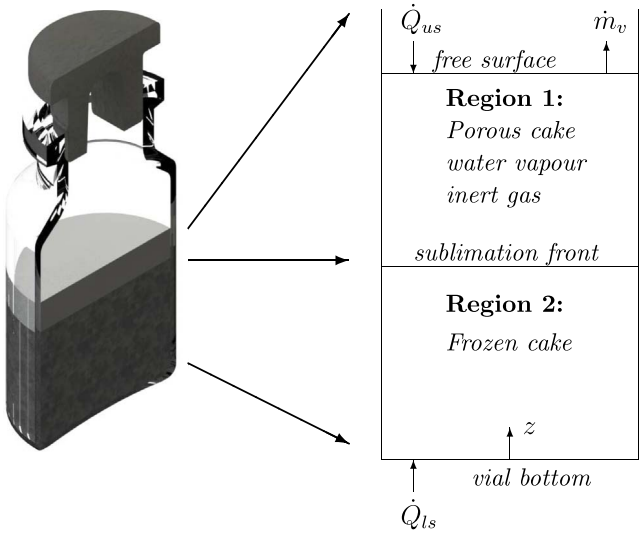

Fig. 1. Typical freeze drying set-up in a vial, one-dimensional approximation.

of the surrounding vials [5]. In the case of fully packed trays in a standard lyophilizer, or additional side plates on the trays, this contribution can be neglected, or its influence distributed to the heat fluxes from the upper and lower shelves, which is especially suitable when using a one-dimensional numerical model, [10–12,14]. Although full 3D or axisymmetrical models can be implemented, lyophilization models based on a one-dimensional approximation of the vial geometry have the advantage of low computational cost, with a comparably accurate solution of heat and mass transfer problem. This becomes extremely important in view of applying a lyophilization model in a vial in the context of Computational Fluid Dynamics simulation of the entire lyophilization system, which can be loaded with several ten thousands of vials. The ability to compute lyophilization dynamics in each of these vials at a low computational cost by applying a one-dimensional model can reduce the overall computational cost of a CFD lyophilization simulation dramatically [2].

3. Experimental procedures and methods

The experiments underlying the numerical model were performed in a laboratory lyophilizer, Christ Epsilon 2–6 D. The measurements were divided into three parts, and repeated in several freeze-drying cycles, in order to provide reliable data for: (i) The temperatures inside the vials, (ii) Temperatures of the drying chamber walls and (iii) Chamber pressure and the temperatures of the condenser and the shelves. The freeze-drying chamber was loaded with 115 vials on each of the three shelves. The Nuova Ompi DIN ISO 10R borosilicate glass vial, with $22mm$ of outer diameter and $1mm$ of glass thickness, was used in the experiments. The vials were filled with 4 ml of the 5 wt% aqueous mannitol solution during the experiments. The temperatures of the product and the walls were measured with an external measuring system comprised of: Thermocouples type T, a data acquisition unit (Agilent 34970A and 34901A) and a personal computer. The absolute expected uncertainty of the temperature measurements was $\pm 2°C$ at the 95% confidence level, employing the coverage factor of 2 in the temperature range from $-45°C$ to $+50°C$. The temperatures of the product inside the vials was measured at three locations along the axis of the vial: $1.5mm$; $5mm$, and $8.5mm$ from the vial's bottom. In order to have quality temperature data, unbiased from the thermocouples support construction, for the comparison with simulation results, the main attention was given to the placement of the thermocouples. As the presence of the support structure could influence the heat transfer conditions inside the material, the thermocouple holder was inserted in the vial to enable a more precise and repeatable positioning of all three thermocouples placed in the vial's axis. A cylindrical zone around the axis with a diameter of at least 10 mm was intruded only with the thin thermocouple wires, as the holder was positioned in the vicinity of the vial's glass wall.

Vials with temperature monitoring were placed in two locations, as is depicted in Fig. 2. The first location is in the centre of the middle shelf, and presents a representative vial, as it is surrounded by other vials; hence, a small effect of the radiation heat transfer from the

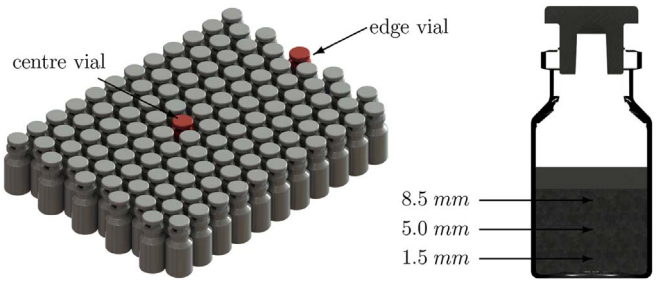

Fig. 2. Positions of the test vials on the tray (left), positions of temperature sensors inside the vial (right).

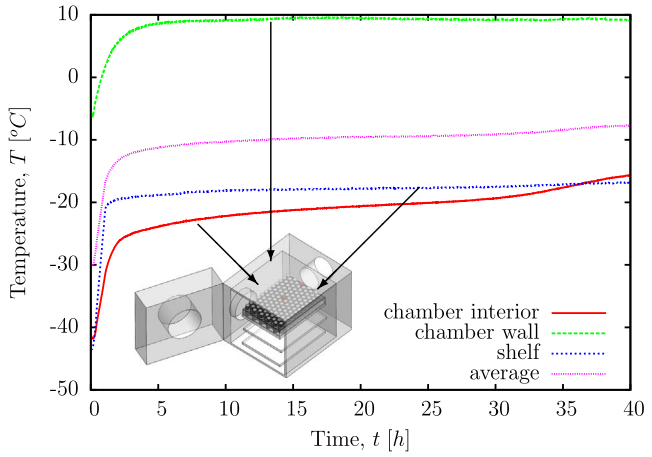

Fig. 3. Temperature measurements used for setting boundary conditions for the centre and the edge vials. The average temperature is calculated using the average of three temperature measurements: The chamber interior, chamber walls and shelf temperature.

chamber walls is expected. The second vial was chosen at the rear edge of the middle shelf, which is adjacent to the wall separating the chamber and the condenser. The selected measured locations made it possible to obtain significantly different drying kinetics of the vials, which result from the non-homogeneous temperature and radiation conditions inside the drying chamber. This is clearly evident from the time plot of the temperature variations of the plate, the walls and the gas, presented in Fig. 3.

The temperature of the walls was measured at several positions in the chamber, typically at two positions along each spatial direction, and then served as data for computation of the overall arithmetic mean of the wall temperatures. Since the used lyophilizer was a laboratory type device, the front doors were transparent with a large blind flange installed in the centre, which could be replaced with a sample retrieving device. Consequentially, the front doors had the worst insulation from the outside air temperature and thermal irradiation to the interior. The side walls of the freeze-drying chamber were not transparent, however, the temperature measurements during the lyophilization process indicate that the thermal insulation was not adequate for a thorough reduction of the heat gains (loss) from the surroundings. Significantly higher temperatures of the walls compared to the temperatures of the shelves were measured during the freezing and the primary drying step of the freeze drying cycle, hence, additional heat gains were affecting especially the edge vials. The process is reversed during the secondary drying step, as the chamber walls are constantly colder than the shelves. Therefore, the heat transfer to the vial was not only influenced by temperature conditions of the shelves, but also by the temperature conditions at the walls.

4. Governing equations

The governing equations for the heat and mass transport phenomena are valid for the volume of the vial occupied by the mannitol-water mixture. The main assumptions of the computational model are considering the frozen region as homogeneous with spatially independent material properties, and the gas phase as a binary ideal gas mixture, which is in thermal equilibrium with the porous cake. At the infinitely thin interface between the frozen and the porous region, the water vapour pressure is in equilibrium with the solid ice phase of the frozen region. At the beginning of lyophilization, the volume consists of the frozen mixture only. With the progression of drying, the upper part of the volume is transformed into a porous structure, while the remainder of the volume stays in the form of a frozen mixture. As in the works of [10] and [18], in order to avoid numerical difficulties associated with moving grid, an initial thickness of the dried region of 2% of the total cake height is prescribed. In order not to use any extrapolation method to account for the consumed drying time for the initial 2% of the domain, a dedicated model is introduced for the sublimation of the surface crystals.

4.1. Conservation of energy

In Region 1, the heat is transferred, due to vapour and inert gas convective fluxes, as well as due to heat conduction, with additional heat sink due to desorption of water from the porous part of the drying substance. The conservation of energy for Region 1 therefore reads as

$$\underbrace{\rho_1 c_{p,1}\frac{\partial T}{\partial t}}_{accumulation} + \underbrace{\vec{\nabla}\cdot((\overrightarrow{N_v}+\overrightarrow{N_i})c_{p,g}T)}_{convection} = \underbrace{\lambda_1\nabla^2 T}_{conduction} + \underbrace{\Delta H_v \rho_{1,p}\frac{\partial C}{\partial t}}_{desorption} \tag{1}$$

In Region 2, the heat transfer mechanism is heat conduction, resulting in the following equation for the conservation of energy:

$$\underbrace{\rho_2 c_{p,2}\frac{\partial T}{\partial t}}_{accumulation} = \underbrace{\lambda_2\nabla^2 T}_{conduction} \tag{2}$$

At the sublimation front, where the frozen and porous part of the domain are in contact, the ice undergoes a phase change, consuming the sublimation enthalpy for this process. At the sublimation front, the frozen region and the porous region have equal temperatures; however, due to different heat conductivities, moving front phenomena and sublimation process, the heat fluxes in both parts of the domain are connected through the following interface condition:

$$\lambda_2\frac{\partial T}{\partial n}\bigg|_2 + \underbrace{v_n\rho_2 c_{p,2}T}_{interface\ term} = \lambda_1\frac{\partial T}{\partial n}\bigg|_1 + \underbrace{v_n\rho_1 c_{p,1}T}_{interface\ term} - \underbrace{\Delta H_s N_{v,n}}_{sublimation} - \underbrace{N_{v,n}c_{p,g}T|_1}_{convection} \tag{3}$$

where the condition $\overrightarrow{N_i}=0$ for the inert gas was considered. The velocity of the sublimation front v_n is computed by

$$v_n = -\frac{N_{v,n}}{\rho_2-\rho_1} \tag{4}$$

Since the one-dimensional approximation of vial geometry is used, the energy conservation equations read as

$$\rho_1 c_{p,1}\frac{\partial T}{\partial t} + \frac{\partial}{\partial z}((\overrightarrow{N_v}+\overrightarrow{N_i})c_{p,g}T) = \lambda_1\frac{\partial^2 T}{\partial z^2} + \Delta H_v\rho_{1,p}\frac{\partial C}{\partial t} \tag{5}$$

for Region 1, and for Region 2

$$\rho_2 c_{p,2}\frac{\partial T}{\partial t} = \lambda_2\frac{\partial^2 T}{\partial z^2}. \tag{6}$$

4.2. Conservation of mass

Conservation of mass needs to be computed only in Region 1, for both water vapour and inert gas, which are treated as ideal gases. Water vapour mass conservation reads as

$$\underbrace{\varepsilon\frac{M_v}{R}\frac{\partial}{\partial t}\left(\frac{p_v}{T}\right)}_{accumulation} + \underbrace{\vec{\nabla}\cdot\overrightarrow{N_v}}_{convection} = -\underbrace{\rho_{1,p}\frac{\partial C}{\partial t}}_{desorption} \tag{7}$$

And inert gas mass conservation is

$$\underbrace{\varepsilon\frac{M_i}{R}\frac{\partial}{\partial t}\left(\frac{p_i}{T}\right)}_{accumulation} + \underbrace{\vec{\nabla}\cdot\overrightarrow{N_i}}_{convection} = 0. \tag{8}$$

The critical part for the performance of the lyophilization models is the correct modelling of water vapour and inert gas mass fluxes. The gradient theory of mass transfer is applied, leading to the expressions:

$$\overrightarrow{N_v} = -\frac{M_v}{RT}(k_1 \vec{\nabla} p_v + k_2 p_v(\vec{\nabla} p_v + \vec{\nabla} p_i)) \tag{9}$$

$$\overrightarrow{N_i} = -\frac{M_i}{RT}(k_3 \vec{\nabla} p_i + k_4 p_i(\vec{\nabla} p_v + \vec{\nabla} p_i)) \tag{10}$$

with diffusivities k_1, k_2, k_3 and k_4 as follow:

$$k_1 = \frac{C_2 D^0_{v,i} K_v}{C_2 D^0_{v,i} + K_{mx}(p_v + p_i)} \tag{11}$$

$$k_3 = \frac{C_2 D^0_{v,i} K_i}{C_2 D^0_{v,i} + K_{mx}(p_v + p_i)} \tag{12}$$

$$k_2 = k_4 = \frac{K_v K_i}{C_2 D^0_{v,i} + K_{mx}(p_v + p_i)} + \frac{C_{01}}{\mu_{mx}} \tag{13}$$

$$K_v = C_1 \sqrt{\frac{RT}{M_v}} \tag{14}$$

$$K_i = C_1 \sqrt{\frac{RT}{M_i}} \tag{15}$$

$$K_{mx} = \frac{p_v}{p_v + p_i} K_v + \frac{p_i}{p_v + p_i} K_i \tag{16}$$

$$D^0_{v,i} = D_{v,i}(p_v + p_i) \tag{17}$$

With insertion of mass flux (10) in equation (8) it follows

$$\varepsilon \frac{M_i}{R} \frac{\partial}{\partial t}\left(\frac{p_i}{T}\right) = \vec{\nabla} \cdot \left(\frac{M_i}{RT}(k_3 \vec{\nabla} p_i + k_4 p_i(\vec{\nabla} p_v + \vec{\nabla} p_i))\right) \tag{18}$$

which, in the case of one-dimensional approximation, reads as

$$\varepsilon \frac{\partial}{\partial t}\left(\frac{p_i}{T}\right) = \frac{k_3}{T}\frac{\partial^2 p_i}{\partial z^2} + (g_3 + g_4)\frac{\partial p_i}{\partial z} + p_i d_4 \tag{19}$$

with

$$\vec{g_3} = \vec{\nabla}\frac{k_3}{T} \tag{20}$$

$$\vec{g_4} = \frac{k_4}{T}(\vec{\nabla} p_v + \vec{\nabla} p_i) \tag{21}$$

$$d_4 = \vec{\nabla} \cdot \left(\frac{k_4}{T}(\vec{\nabla} p_v + \vec{\nabla} p_i)\right) = \vec{\nabla} \cdot \vec{g_4} \tag{22}$$

As at the sublimation interface, the mass flux of the inert gas is $N_i = 0$, the following boundary condition for the inert gas pressure at the interface is valid:

$$p_i^{(1)} = \frac{p_i^{(2)}}{1 - \frac{k_4 \Delta z}{k_3}(\vec{\nabla} p_v + \vec{\nabla} p_i)}. \tag{23}$$

With insertion of the mass flux of water vapour (9) into the vapour mass conservation equation (7), it follows

$$\varepsilon \frac{M_v}{R} \frac{\partial}{\partial t}\left(\frac{p_v}{T}\right) = \vec{\nabla} \cdot \left(\frac{M_v}{RT}(k_1 \vec{\nabla} p_v + k_2 p_v(\vec{\nabla} p_v + \vec{\nabla} p_i))\right) - \rho_{1,p}\frac{\partial C}{\partial t} \tag{24}$$

which, in the one-dimensional approximation reads as

$$\varepsilon \frac{\partial}{\partial t}\left(\frac{p_v}{T}\right) = \frac{k_1}{T}\frac{\partial^2 p_v}{\partial z^2} + (g_1 + g_2)\frac{\partial p_v}{\partial z} + p_v d_2 - \frac{R}{M_v}\rho_{1,p}\frac{\partial C}{\partial t} \tag{25}$$

with

$$\vec{g_1} = \vec{\nabla}\frac{k_1}{T} \tag{26}$$

$$\vec{g_2} = \frac{k_2}{T}(\vec{\nabla} p_v + \vec{\nabla} p_i) \tag{27}$$

$$d_2 = \vec{\nabla} \cdot \left(\frac{k_2}{T}(\vec{\nabla} p_v + \vec{\nabla} p_i)\right) = \vec{\nabla} \cdot \vec{g_2} \tag{28}$$

On the free surface, the water vapour partial pressure is set to bulk vapour partial pressure

$$p_v^{(n)} = p_v^0 \tag{29}$$

whereas, on the sublimation interface during the primary drying, the vapour pressure is set to the saturation water vapour pressure at the temperature of the interface,

$$p_i^{(1)} = p_v^\star. \tag{30}$$

The partial pressure of saturation depends on the interaction of the freeze drying material and ice, as well as on the temperature, and has the following form:

$$p_v^\star = B_1 \cdot \exp\left(B_2 - \frac{B_3 \Delta H_v}{T}\right) \tag{31}$$

where B_1, B_2 and B_3 are model constants that depend on the composition of the freeze drying material. With the onset of the secondary drying phase, the condition $N_v = 0$ holds at the bottom of the vial, which results in the following boundary condition for the water vapour pressure condition at the vial bottom:

$$p_v^{(1)} = \frac{p_v^{(2)}}{1 - \frac{k_2 \Delta z}{k_1}(\vec{\nabla} p_v + \vec{\nabla} p_i)}. \tag{32}$$

In the second drying phase, the desorption process takes place in the already dried region during the drying process on the surface of the porous solid structure. For the mass conservation equations (7) and (8), the rate of desorption has to be determined. In this case, the first order kinetics model was used,

$$\frac{\partial C}{\partial t} = k_g(C^\star - C), \tag{33}$$

where k_g represents the mass transfer coefficient and $C^\star$ the equilibrium water concentration, which depends on the partial pressure of the water vapour, the amount of bounded water inside the dried material, and temperature. For the equilibrium water concentration the following form was implemented:

$$C^\star = A_1 \cdot \exp(A_2(A_3 - A_4 \cdot (T - T_0))) \tag{34}$$

where A_1, A_2 and A_3 are the binary mixture constants, and T_0 the initial temperature of the frozen material.

4.3. Model of surface sublimation

As mentioned, an initial thickness of the dried region of 2% of the total cake height is used when starting the numerical solution of conjugate heat and mass transfer in the porous-frozen layer system. A dedicated model for the sublimation of the surface crystals is needed In order to account for the consumed drying time for the initial 2% of the domain. From the SEM analysis, a typical size of the ice crystals is in the order of $200\mu m$, which equates approximately to 2% of the height of the cake. If we simplify the conditions at the free surface to a single layer of ice crystals, the sublimation model of ice crystals can be designed with a direct contact with the fluid space of the vial.

The case of sublimating ice crystals can be modelled as one-sided diffusion of water vapour from the layer of ice crystals in the direction of the vial opening, in the form of [3]:

$$\vec{J}'_v = \frac{C_v}{C_v + C_i}\vec{J}'_v - \mathscr{D}_{v,i}\vec{\nabla} C_v.$$

In the direction z, perpendicular to the ice surface layer the molar flux of vapour is

$$J'_v = \frac{C_v}{C_v + C_i} J'_v - \mathscr{D}_{v,i} \frac{dC_v}{dz}.$$

By considering that the temperature in the interior of the vial fluid volume is not varying significantly, and by using the ideal gas law

$$p_v = C_v RT \tag{35}$$

the molar flux (35) reads as

$$J'_v = \frac{p_v}{p_v + p_i} J'_v - \frac{\mathscr{D}_{v,i}}{RT} \frac{dp_v}{dz}. \tag{36}$$

The vapour diffusivity in the binary mixture is taken according to [20] as:

$$\mathscr{D}_{v,i} = 0.01883 \frac{\sqrt{T^3 \left(\frac{1}{M_v} + \frac{1}{M_i}\right)}}{(p_i + p_v)\sigma_{vi}^2 \Omega_D} \tag{37}$$

The Lennard-Jones parameters for the binary mixture are

$$\sigma_{vi} = \frac{\sigma_v + \sigma_i}{2}, \qquad \varepsilon_{vi} = \sqrt{\varepsilon_v \varepsilon_i}. \tag{38}$$

with parameter Ω_D the collision integral. By inserting Eq. (37) into Eq. (36), it follows

$$p_i J'_v = -0.01883 \frac{\sqrt{T\left(\frac{1}{M_v} + \frac{1}{M_i}\right)}}{R\sigma_{vi}^2 \Omega_D} \frac{dp_v}{dz}. \tag{39}$$

To get the molar flux, integration is needed from the sublimation surface ($p_{v,0} = p_v^*$) to the top of the vial with conditions of the free space of the lyophilizer drying chamber ($p_{v,h}$),

$$J'_v \int_0^h dz = -0.01883 \frac{\sqrt{T\left(\frac{1}{M_v} + \frac{1}{M_i}\right)}}{p_i R\sigma_{vi}^2 \Omega_D} \int_{p_{v,0}}^{p_{v,h}} dp_v$$

resulting in the final expression for the molar flux

$$J'_v = -0.01883 \frac{\sqrt{T\left(\frac{1}{M_v} + \frac{1}{M_i}\right)}}{p_i R\sigma_{vi}^2 \Omega_D} \frac{p_{v,h} - p_{v,0}}{h} \tag{40}$$

With known J'_v the time for drying of the first 2% of the cake height (Δh), can be computed as:

$$\Delta t = \frac{\rho_1 \Delta h}{M_v J'_v} \tag{41}$$

4.4. The effect of the porous structure on mass transfer

The effective diffusivity terms $k_1 \ldots k_4$ include the Fick's diffusivities, as well as the effect of the Knudsen diffusivity in the parameters K_v and K_i, playing an important role in mass transfer at the micro scale and under conditions of extremely low pressure. In the case in lyophilization, the system pressure is at the level of $10Pa$ and a typical dimensional scale of the porous structure is $10 - 200\mu m$, so the Knudsen diffusivity plays an important role in the mass transfer resistance of the porous structure.

The general model of the Knudsen diffusivity reads as

$$K_{kn} = \frac{\lambda}{3} \sqrt{\frac{8RT}{\pi M}} \tag{42}$$

with λ the molecular free path. For the porous layer, it is reasonable to assume that the free path of the molecules is of the same magnitude as the pore diameter, i.e. $\lambda = d_p$, resulting in

$$K_{kn} = \frac{d_p}{3} \sqrt{\frac{8RT}{\pi M}} \tag{43}$$

As we are dealing with the porous structure of the dried cake, where porosity ε and tortuosity τ influence the diffusive transport process, the effective diffusivity concept can be applied:

$$K_{eff} = \frac{\varepsilon}{\tau} K_{kn} \tag{44}$$

Leading to

$$K_{eff} = \frac{\varepsilon}{\tau} \frac{d_p}{3} \sqrt{\frac{8RT}{\pi M}} \tag{45}$$

As the lyophilization model uses the diffusivity in the following form, see Eqs. (14) and (15),

$$K_v = C_1 \sqrt{\frac{RT}{M_v}}, \qquad K_i = C_1 \sqrt{\frac{RT}{M_i}} \tag{46}$$

the following dependence is obtained of the model parameter C_1 on the geometrical properties of the porous layer:

$$C_1 = \frac{\varepsilon}{3\tau} \sqrt{\frac{8}{\pi}}\, d_p \tag{47}$$

From the SEM analysis, the typical pore dimensions of the lyophilized 6% mannitol solution are in the range $150 - 200\mu m$ [17]. However, in the work of [7]; results of the pore diameter of $13\mu m$ for 5% mannitol solution in the case of the freezing step with uncontrolled nucleation was reported, determined on the basis of measurement of the mass transfer resistance and the use of the Knudsen model for the diffusivity. The results indicate that not only the size of the dry cake pore plays an important role, but also the fact that nucleation produces large, predominantly closed cake pores. The Knudsen diffusivity takes place in the openings of these pores, which are, typically, one magnitude smaller than the cake pore. In view of these findings, the pore diameter applied in the computational model of lyophilization, was selected as $d_p = 15\mu m$. The porosity of the dry cake was estimated at 0.95, and tortuosity at $\sqrt{3}$, leading to the value of $C_1 = 4.4\mu m$. As one value of C_1 represents the whole pore structure with a clearly nonuniform pore size distribution, it is, of course, not possible to determine experimentally an exact value of the representative pore diameter. The correct value of the C_1 in the computational model should, therefore, be determined through a sensitivity analysis based on a comparison with test experimental results of lyophilization for the targeted drying material and the implemented freezing step protocol.

5. Computational model

The governing equations of heat and mass conservation for the one-dimensional approximation of the vial were discretized by using the Finite Difference Method. The central differencing scheme was used for spatial derivatives, and the backward Euler scheme for the temporal derivatives. The one-dimensional approximation was chosen in order to keep the computing time as short as possible, since we intend to use of this model as a sub-model for a full 3D simulation of production lyophilizers having hundreds of vials all running this model.

A grid independence study was performed for the case of skim milk lyophilization [10]. The same computational model was used, meaning that the simulation starts with the initial porous layer at the top of 2% of the cake height. The computational grids with 50 and 100 grid points were tested, and time step values of $0.1s$ and $1s$. The comparison of obtained results showed that the computational grid with 50 points, evenly distributed between the solid and porous part of the domain, for both time step values predicted the spatial variation of field variables adequately. In the case of time step analysis the time step value of $1s$ was chosen, as it allowed relatively short computation times.

The numerical simulations of mannitol solution lyophilization were, therefore, performed by using 50 grid points and $1s$ time step. The initial height of the cake was $L = 0.0115m$. The start of the one-dimensional model was at the $z_{intf,start} = 0.98L$, and the introduced surface sublimation model was used in order to account for the drying of the

Table 1
The boundary conditions for the vial.

	Bottom	Side	Top	Subl. interface
Energy - region 1	/	$U_s = 0$	Eq. (48)	Eq. (3)
Energy - region 2	Eq. (48)	$U_s = 0$	/	Eq. (3)
Mass - p_v	/	$\overrightarrow{N_v} = 0$	$p_v = 5Pa$	Eq. (30)
Mass - p_i	/	$\overrightarrow{N_i} = 0$	$p_i = 4Pa$	$\overrightarrow{N_i} = 0$

upper 2% of the cake height. At the bottom, when the sublimation interface reached 2% of the total height, the primary drying phase simulation was continued using a simple linear algebraic model [10], with extrapolated drying kinetics by using the last one-dimensional computed drying rate for the computation of the removal of the bottom 2% of the ice.

5.1. Initial and boundary conditions, material parameters

The initial conditions for the temperature were taken to be $T_0 = 231K$, while for the partial pressure of the inert gas $p_{i,0} = 4Pa$, and partial pressure of the water vapour $p_{v,0} = 7Pa$. The initial total pressure in the dried region is then $p_0 = p_{i,0} + p_{v,0} = 11Pa$, which is equal to the pressure in the lyophilization chamber. The concentration of absorbed water in the dried region was set according to the model for $C^\star$ in Table 2.

For the boundary conditions, we have to prescribe the boundary conditions for all boundaries and for all three variables, temperature, partial pressure of inert gas and water vapour. The overall heat flux density $\dot{q}$ is proportional to the overall heat transfer coefficient U and temperature difference between the boundary condition of the shelf or wall T_{bc} and vial temperature T_v,

$$\frac{dq}{dt} = U(T_{bc} - T_v)\,, \tag{48}$$

In the presented model, the U includes all heat transfer mechanisms: Conduction, radiation and convection.

As the numerical model used in the simulation is one-dimensional, the vial sidewall boundary conditions were set as adiabatic. Therefore, the 1D numerical model includes two vial surfaces, where heat is supplied to the vial: The bottom and the top surface. At the top surface, the heat radiation from the upper shelf, as well as from the chamber walls, governs the supplied heat flux. The product is partially shielded due to the presence of the stopper. At the bottom, a combination of heat radiation in the gap between the vial bottom and the shelf, and heat conduction takes place at the contact area with the shelf. The specification of the T_{bc} temperature in Eq. (48) depends on the chosen surface. For the case of the centre and edge vials, the shelf temperature is set as the temperature boundary condition. At the top surface, the T_{bc} temperature does depend on the position of the vial on the shelf. The centre vial, used for validation of computational results, and depicted in Fig. 2, is located in the mid shelf, surrounded by other vials, and the upper shelf, therefore the shelf temperature is set as the T_{bc} temperature in the model (48).

The comparison of the measurements of the temperature conditions in the chamber (Fig. 3) and measurements of dry cake temperatures (Figs. 9 and 10) shows that, for the centre vial at the end of the experiment, the measured dry cake temperature is higher than the shelf temperature by $0.8°C$, indicating the presence of surfaces with higher temperatures than the temperatures of the shelves. Additionally, in the case of the edge vials, sublimation dynamics are clearly different to the centre vials. As a laboratory type lyophilizer was used for experimental testing, a check on the temperature conditions at the chamber walls was made. The temperature measurements in the lyophilizer chamber during the majority of the primary drying step showed that the temperature of the side walls was at approx. 10°C, while the shelf temperature was at approx. -20°C, see Fig. 3. Therefore, the significant effect of the side walls was established. The edge vials are, therefore, exposed to heat radiation at much higher radiation temperatures than the centre vials. The effect of the chamber walls' radiation was then accounted for by a modification of the wall temperature (T_{bc}) in the heat transfer boundary condition (48) at the top surface of the edge vial, whereas the boundary conditions for the bottom of the vial were set the same as in the centre vial position. For the edge vial, the sidewall effect was taken into account at the top surface by using a modified temperature boundary condition, set to the average temperature of the gas, the chamber side walls and the shelf, see Fig. 3. In the work of [6]; heat transfer coefficient values were reported, defined on the outer cross-sectional area of the vial, of $16W/m^2K$ for the centre vial, and $26W/m^2K$ for the edge vial. In our case, in order to account for different radiation conditions at the centre and edge positions, and also to account for the boundary conditions that are imposed on the inner cross-sectional area of the vial, the heat transfer coefficient for the top surface was set to $U_{up} = 1W/m^2K$ at the centre position, and $U_{up} = 16W/m^2K$ at the edge position. A separate in-depth analysis of the heat transfer from the chamber surroundings to the interior of the drying chamber would be needed in order to determine local temperatures of the walls, which would then serve as a basis for a more accurate setting of the heat transfer boundary conditions for drying of the edge vials. At the vial bottom, the heat transfer conditions at the centre and edge vials were assumed to be equal, and were set as $U_{lp} = 16W/m^2K$. T_{bc} was used for the temperature of the shelf. At the onset of the secondary drying phase, the conditions at the bottom of the vial change, as the ice/glass contact is replaced by porous cake/glass contact, which is included in the model by imposing the $U_{lp} = 1W/m^2K$. If another vial material or another vial form is used, this could affect the heat transfer coefficient values. In this case, the change in the glass thermal conductivity and emmissivity, as

Table 2
Value and models of different variables for 5% mannitol-water solution.

Variable	Value or model
$C_{01}[m^2]$[18]	$7.219{\cdot}10^{-15}$
C_2[10]	0.4428
C^*[10]	$0.01\exp(2.3(1.36 - 0.036(T - T_0))$
$c_{p,g}[J/kgK]$	1674.7
$c_{p,1}[J/kgK]$	1715
$c_{p,2}[J/kgK]$	2054
$D^0_{v,i}[kg/ms^3]$[18]	$0.00014931(T^3(1/M_v + 1/M_i))^{0.5}$
$\in$	0.95
$\Delta H_v[kJ/kg]$[16]	2840.2
$\Delta H_s[kJ/kg]$[16]	2687.4
$k_g[s^{-1}]$[10]	$11.08{\cdot}10^{-5}$
k_2, k_4	0
$k_B[m^2kgs^{-2}K^{-1}]$	$1.38064852{\cdot}10^{-23}$
$\lambda_1[W/mK]$[10]	$680(12.98{\cdot}10^{-8}(p_i + p_v) + 39.806{\cdot}10^{-6})$
$\lambda_2[W/mK]$	2.661
$\lambda_{solid}[W/mK]$	0.1
$M_i[kg/kmol]$	29
$M_v[kg/kmol]$	18
$\mu_{mx}[kg/ms]$[18]	$[18.4858(T^{1.5}/(T + 650))]$
$p_v^\star[Pa]$[10]	$133.32{\cdot}\exp\left(23.9936 - \frac{2.19\Delta H_v}{T}\right)$
$\rho_{solid}[kg/m^3]$	1500
$\rho_{1,p}[kg/m^3]$	75.0
$\rho_2[kg/m^3]$	952.8
$\rho_I[kg/m^3]$	924
$\rho_1[kg/m^3]$	260
$R[J/kmolK]$	8314
σ_i[Å][3]	3.771
σ_v[Å][3]	3.737
$\varepsilon_v/k_B[K]$[3]	32
$\varepsilon_{vi}/k_B[K]$[3]	50

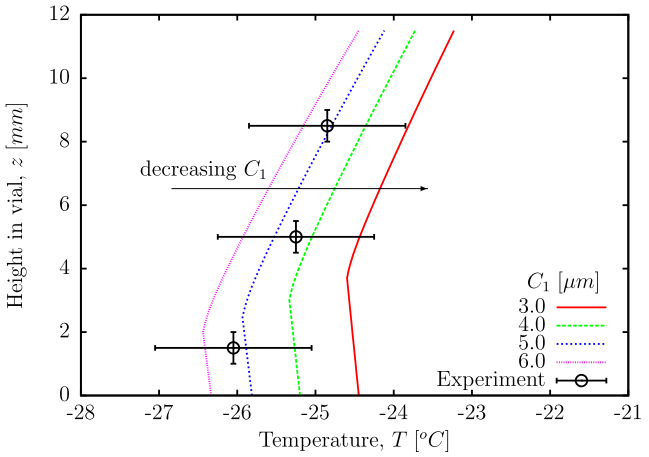

Fig. 4. Temperature profiles after $25h$ of primary drying for different values of C_1.

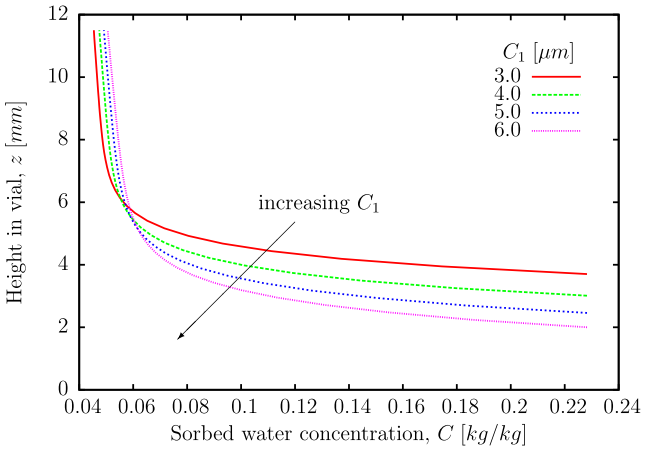

Fig. 5. Concentration profiles after $25h$ of primary drying for different values of C_1.

well as a different vial bottom geometry, would need to be accounted for in determination of the corrected heat transfer values. The prescribed boundary conditions for energy and mass transfer equations are summarised in Table 1.

The material properties, the used models and model parameters are summarised in Table 2. The material properties are valid for the 5% mannitol-water solution, except where referenced on previous works of [10] and [18].

6. Computational results and discussion

The derived numerical model of lyophilization of mannitol solution in a vial was validated using data from the performed experiments. Computational results were validated using the experimental data on drying for two vial positions, as depicted in Fig. 2.

Since the accuracy of the computational model is, to a large extent, based on the selection of physical models, a dedicated sensitivity analysis was performed. As the lyophilization is a diffusion driven process, special attention was devoted to the correct modelling of this process. A typical lyophilization configuration consists of the partially dried porous cake in contact with the frozen bottom layer, and the drying rate depends strongly on the resistance of the dried region to the water vapour diffusion. As the main modelling parameter influencing the diffusion process in the porous layer is the C_1 (Eq. (47)) its value depends on the size of a typical pore of the porous cake, the sensitivity analysis of the C_1 value, and its influence on the drying kinetics of mannitol solution was performed. The computed value of $C_1 = 4.4\mu m$ was, therefore, varied in the range $3.0 - 6.0\mu m$, and computations were performed for the case of the centre vial.

From the temperature profiles along the central axis, presented in Fig. 4, it is evident that a lower value of C_1 leads to lower drying rates, as the interface position, denoted by a knickpoint in the temperature profile, is higher than in the case of higher values of C_1.

The higher value of C_1 leads to higher diffusion rates through the porous cake, which promote drying intensity and, in consequence, also increase the intensity of the heat sink at the interface due to the increased sublimation rate. A consequence of this increase is lower temperature values in the vial, that also influence the water concentration profiles. In the case of concentration profiles, a higher value of C_1 and, consequently, higher sublimation rate, leads to lower concentration values in the porous cake in the vicinity of the sublimation front. On the other hand, as a higher sublimation rate decreases temperature level inside the vial, this influences the desorption rate negatively, Eq. (34), hence the concentration of water in the upper part of the porous region decreases faster in the case of lower C_1 values, Fig. 5. In the secondary phase of drying, the higher sublimation rates of the primary phase in the case of a high C_1 value result in an earlier onset of the secondary phase and faster increase in temperature level inside the vial, leading to a faster decrease of the sorbed water concentration in the porous cake, as can be concluded from Fig. 6, presenting concentration profiles at the elapsed time of $45h$.

Especially important for lyophilization procedure development is the correct computation of the interface position and its temporal development, as the end of the primary phase, when the interface position reaches the value of $0\ mm$, allows an increase of the shelf temperature for the onset of the secondary drying. From the time histories of interface position for various C_1 values, one can observe clearly that the increase in C_1 leads to faster interface movement and shorter primary phase drying times. As a correct determination of the primary phase end is especially important, a choice of $C_1 = 5.0\mu m$ leads to the most accurate computational results in the final stages of the primary phase, see Fig. 7. This, together with the analysis of the temperature profiles in Fig. 4, led to the decision of selecting the $C_1 = 5.0\mu m$ as the model value used for the further analysis of the drying kinetics of the mannitol-water solution.

The sublimation front position as a function of time is shown in Fig. 8 for both the centre and the edge vials. The experimental determination of sublimation front position was obtained by examining the temperature time traces, even though the presence of temperature probes disrupts the sublimation front. It is evident that the computational results of the sublimation interface tracking are in good agreement, and yield a slightly higher position of the interface compared to the measured values. The source of this disagreement between the measured and modelled sublimation front position could be an initially larger variation of thermal conditions in the chamber, which is not

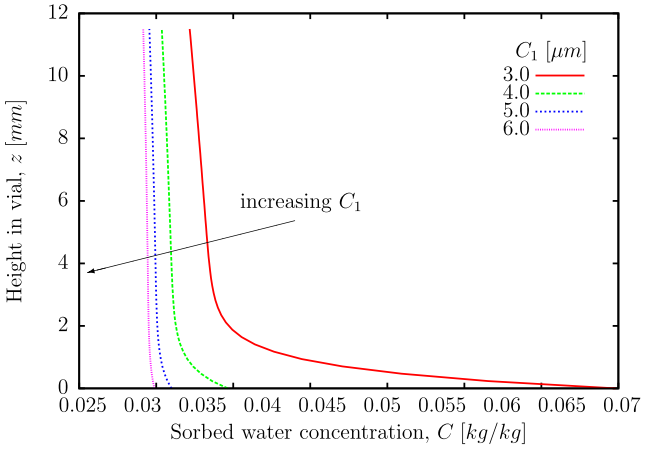

Fig. 6. Concentration profiles in the secondary drying phase, at the time of $45h$, for different values of C_1.

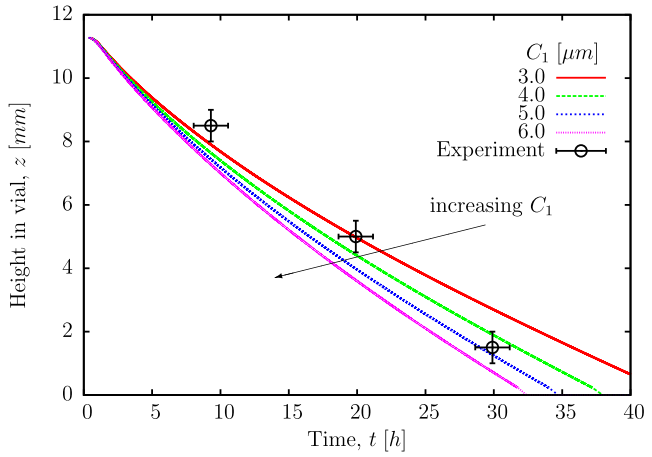

Fig. 7. Dependence of the temporal development of the sublimation interface position on the variation of effective Knudsen diffusivity for the case of centre vial.

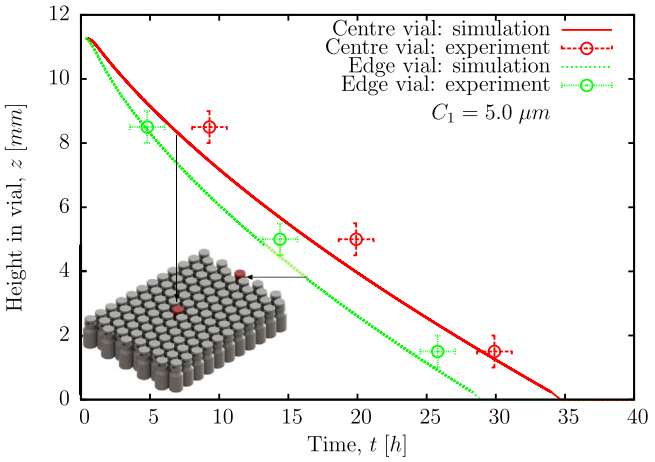

Fig. 8. Comparison between experimental and numerical movement of sublimation interface position for the cases of the centre and edge vials.

covered by imposing constant boundary conditions. This is more evident in the starting phase of the primary phase, which is characterised by an increase of the tray temperature. Additionally, the start of the primary phase is characterised by the decrease of the system pressure, which is also not covered by the imposed boundary conditions. Since the interface position in both vial cases lies below the experimentally determined positions, setting up a transition boundary conditions for the first part of the primary drying could be one of the possible modelling solutions, which would require a more in-depth experimental study of thermodynamic conditions that occur in the early stage of the primary drying phase.

The drying kinetics of the primary phase, and the transition to the secondary phase, are depicted in Fig. 9 for the centre vial, and in Fig. 10 for the edge vial. Comparison of experimental and modelled temperature shows good agreement ($\pm$ 1°C) for the centre vial and poorer agreement for the edge vial ($\pm$ 2°C). This shows that the chosen 1D model is less appropriate for the edge vial, where the heat transfer processes from the side are more pronounced.

Especially important are the transition points at the sensor positions (z value), denoting the end of ice sublimation at the location of the sensor, and the onset of desorption drying in the porous cake, which are characterised by a significantly increasing temperature.

After all the ice in a vial is removed, i.e. at the sublimation end (See Figs. 9 and 10), the second drying phase is initiated, characterised by a strong increase in the temperature. In Tables 3 and 4, the comparison of transition points in time, together with accompanying temperatures for

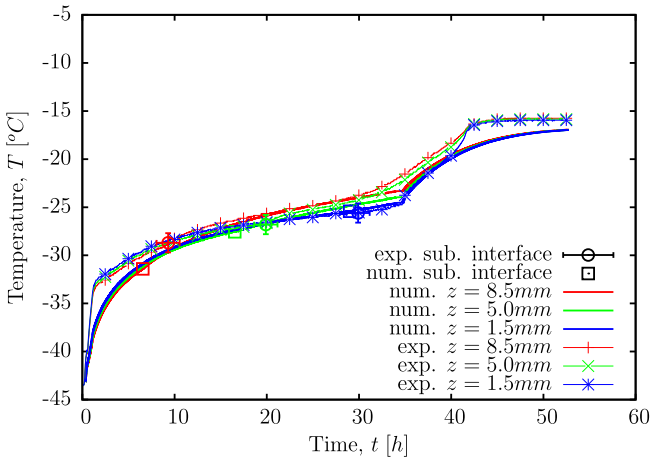

Fig. 9. Centre vial: Temperature development at level $z = 8.5mm$, $5.0mm$ and $1.5mm$ with sublimation interface positions, denoted with squares for numerical values and circles for experimental values.

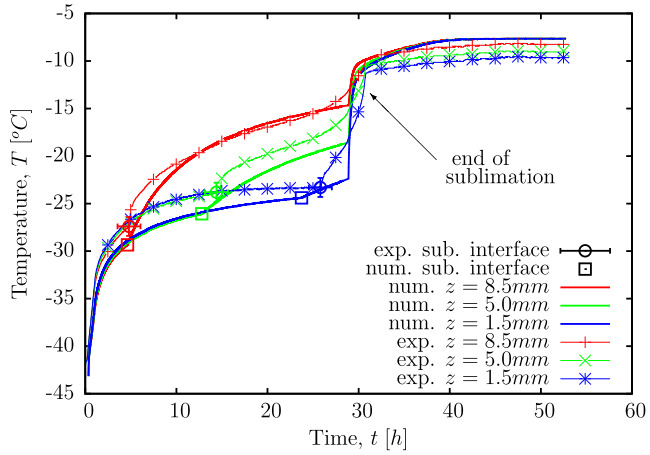

Fig. 10. Edge vial: Temperature development at level $z = 8.5mm$, $5.0mm$ and $1.5mm$ with sublimation interface positions, denoted with squares for numerical values and circles for experimental values.

Table 3
Sublimation interface dynamics data for the centre vial.

Sensor height z [mm]	8.5	5.0	1.5
Time experiment [h]	9.3	19.9	29.9
Time simulation [h]	6.7	16.5	29.0
Temperature experiment [°C]	−28.7	−26.8	−25.6
Temperature simulation [°C]	−31.4	−27.5	−25.4

Table 4
Sublimation interface dynamics data for the edge vial.

Sensor height y [mm]	8.5	5.0	1.5
Time experiment [h]	4.8	14.4	25.8
Time simulation [h]	4.6	12.8	23.7
Temperature experiment [°C]	−27.4	−23.8	−23.3
Temperature simulation [°C]	−29.3	−26.1	−24.4

different vertical positions in the vial, is presented. In the listing of drying times the additional time for drying of the upper surface layer was included with 1277s for drying of the upper surface layer, as well as additional 2460s for drying of the ice layer at the bottom of the vial. As already discussed, the agreement is good for the case of the centre vial and very good for the case of the edge vial.

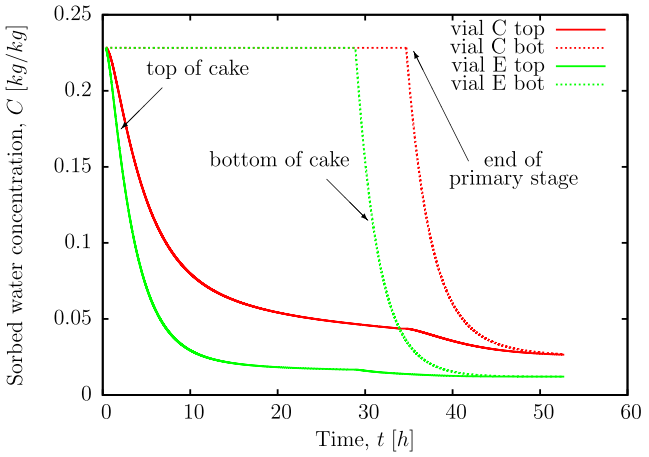

Fig. 11. Concentration development at the top and at the bottom of the cake (C for centre and E for edge vial) for the primary and secondary drying phases.

Further interesting information can be extracted from the dynamics of water concentration near the top of the cake (at $y = 0.98L$) and near the bottom of the vial (at $y = 0.02L$). After a different concentration history in the primary phase, a result of the moving sublimation interface and associated heat sink, in the secondary phase, the temperatures, as well as concentrations near the top and near the bottom, converge towards the final equilibrium state, as depicted in Fig. 11. The difference in the end concentrations is the result of different thermal conditions for the edge and the centre vials, which influence the equilibrium concentration value directly, Eq. (34).

It is also possible to apply the developed numerical model to other types of materials. The heat conduction in the frozen phase is prescribed completely when the physical properties of the frozen phase are known. For this part, the mixture model could be used in determination of the mixture properties, where the properties of each species and their mass fractions are the input to the model. In the case of the transport properties of the porous part of the lyophilization cake, the main parameter to be determined correctly for a different type of material is the typical pore dimension of the cake. To determine this parameter, one lyophilization cycle must be performed experimentally with the new material type. The obtained lyophilization cake then needs to be analysed with the Scanning Electron Microscopy procedure, to determine the average pore size, and to compute the C_1 value according to Eq. (47). As through SEM analysis determined pore size is only a representative value, the value of the C_1 should be corrected through the sensitivity analysis of the influence of the C_1 value on the computed temperature dynamics at the bottom of the vial filling, which has to as close as possible to the experimentally obtained temperatures. As the cake porosity depends on thermodynamic conditions during the freezing step, there is, in general, a difference in the cooling dynamics between the layers close to the edges of the filling and the interior of the vial, which can lead to spatially varying pore sizes. In case there is reliable data on the spatial variation of the porous structure, a spatial variation of the representative value of the pore size could be derived and implemented in the proposed computational model without the need to change the model, as all the material properties are defined on a local basis, i.e. they can vary from grid point to grid point.

The described model implementation procedure should be done for one set of system parameters, i.e. one setting of system pressure and shelf temperature in the primary drying, and the obtained material parameters can then be used for computational studies of the influence of different system pressure values and shelf temperature protocols on the lyophilization of the selected material. Furthermore, it has to be noted that the developed model is suitable for use in all the lyophilization cases where there is change in the porous structure of the upper part of the cake change during the primary drying cycle. Finally, as reported already in Ref. [8], the governing equations can be extended to account also for drying of amorphous solutes by additional consideration of surface diffusion of sorbed water in the porous cake, as well as solid diffusion of water inside the amorphous solids.

7. Conclusions

The development of optimal lyophilization procedures for different formulations in vials increasingly includes a combination of experimental tests and computational approaches. In order to decrease the number of experimental tests, computational approaches should be capable to track the temporal, as well as spatial development of temperature and concentration fields inside a vial accurately. As the final goal of computational approaches is a combination of computational sub-models for drying in vials with the Computational Fluid Dynamics (CFD) approaches for computation of spatial variations of flow field, temperature and species concentrations, the computational models based on one-dimensional approximation of a vial are one of the faster possible solutions. With the use of simple front tracking algorithms, one typically starts the computation with an existing, pre-defined thin porous (surface) layer at the top of the cake, as well as ends it with extrapolation of drying curves for the bottom thin ice layer. In order to include the removal of the surface layer into the numerical model, a dedicated surface sublimation model was developed, based on a one-sided diffusion model. In the computational case of 5% mannitol-water solution, studied in this work, this typically resulted in an additional $0.35h$ of drying time.

Since the critical part of any lyophilization procedure is the primary drying phase, special attention has to be devoted to critical modelling parameters of drying of a porous cake-solid ice system. Strong dependence of sublimation rate on vapour diffusion through the porous layer can be included into the modelling framework by a dedicated sub-model of the C_1 modelling parameter, based on the Knudsen diffusivity, which was linked to the typical pore diameter of the porous cake. A sensitivity analysis showed that the value of $C_1 = 5.0\mu m$ for the porous cake of mannitol leads to very good agreement of the final computational results. Finally, a special emphasis was also paid to thermal conditions in the applied laboratory scale lyophilizer, a type often used in pharmaceutical pre-production procedures. A strong dependence of thermal boundary conditions on the temperatures of the inner walls of the drying chamber was established, and, in the case of the vials at the tray edges, a modified bulk temperature definition was included into the model of boundary conditions.

The developed one-dimensional model with surface sublimation sub-model can be used as a stand alone, fast and accurate computational tool for prediction of lyophilization dynamics, but can also be included into a general 3D CFD computational framework as a vital part of the final virtual lyophilizer model.

Conflicts of interest

The authors report no conflicts of interest. The authors alone are responsible for the content and writing of the paper.

References

[1] A.A. Alexeenko, A. Ganguly, S.L. Nail, Computational analysis of fluid dynamics in pharmaceutical freeze-drying, J. Pharmaceut. Sci. 98 (9) (2009) 3483–3494.
[2] A.A. Barresi, R. Pisano, V. Rasetto, D. Fissore, D.L. Marchisio, Model-based monitoring and control of industrial freeze-drying processes: effect of batch non-uniformity, Dry. Technol. 28 (5) (2010) 577–590.
[3] R.B. Bird, W.E. Stewart, E.N. Lightfoot, Transport Phenomena, Wiley, 2007.
[4] M. Brülls, A. Rasmuson, Heat transfer in vial lyophilization, Int. J. Pharm. 246 (1) (2002) 1–16.
[5] K.H. Gan, R. Bruttini, O.K. Crosser, A.I. Liapis, Freeze-drying of pharmaceuticals in vials on trays: effects of drying chamber wall temperature and tray side on lyophilization performance, Int. J. Heat Mass Tran. 48 (9) (2005) 1675–1687.
[6] V. Koganti, E. Shalaev, M. Berry, T. Osterberg, M. Youssef, D. Hiebert, F. Kanka,

M. Nolan, R. Barrett, G. Scalzo, G. Fitzpatrick, N. Fitzgibbon, S. Luthra, L. Zhang, Investigation of design space for freeze-drying: use of modeling for primary drying segment of a freeze-drying cycle, AAPS PharmSciTech 12 (3) (2011) 854–861.
[7] A. Konstantinidis, W. Kuu, L. Otten, S. Nail, R. Sever, Controlled nucleation in freeze-drying: effects on pore size in the dried product layer, mass transfer resistance, and primary drying rate, J. Pharmaceut. Sci. 100 (8) (2011) 3453–3470.
[8] A. Liapis, R. Bruttini, Freeze-drying of pharmaceutical crystalline and amorphous solutes in vials: dynamic multi-dimensional models of the primary and secondary drying stages and qualitative features of the moving interface, Dry. Technol. 13 (1–2) (1995) 43–72.
[9] R. Litchfield, A.I. Liapis, An adsorption-sublimation model for a freeze dryer, Chem. Eng. Sci. 34 (9) (1979) 1085–1090.
[10] W. Mascarenhas, H. Akay, M. Pikal, A computational model for finite element analysis of the freeze-drying process, Comput. Meth. Appl. Mech. Eng. 148 (1) (1997) 105–124.
[11] W. Massey, J. Sunderland, Heat and mass transfer in semi-porous channels with application to freeze-drying, Int. J. Heat Mass Tran. 15 (3) (1972) 493–502.
[12] M. Millman, A. Liapis, J. Marchello, An analysis of the lyophilization process using a sorption-sublimation model and various operational policies, AIChE J. 31 (10) (1985) 1594–1604.
[13] M. Petitti, A.A. Barresi, D.L. Marchisio, Cfd modelling of condensers for freeze-drying processes, Sadhana 38 (6) (2013) 1219–1239.
[14] M. Pikal, M. Roy, S. Shah, Mass and heat transfer in vial freeze-drying of pharmaceuticals: role of the vial, J. Pharmaceut. Sci. 73 (9) (1984) 1224–1237.
[15] H. Sadikoglu, A. Liapis, Mathematical modelling of the primary and secondary drying stages of bulk solution freeze-drying in trays: parameter estimation and model discrimination by comparison of theoretical results with experimental data, Dry. Technol. 15 (3–4) (1997) 791–810.
[16] P. Sheehan, A.I. Liapis, Modeling of the primary and secondary drying stages of the freeze drying of pharmaceutical products in vials: numerical results obtained from the solution of a dynamic and spatially multi-dimensional lyophilization model for different operational policies, Biotechnol. Bioeng. 60 (6) (1998) 712–728.
[17] A. Sitar, K. Škrlec, J. Voglar, M. Avanzo, M. Kočevar, M. Cegnar, Š. Irman, J. Ravnik, M. Hriberšek, I. Golobič, The effects of controlled nucleation on freeze-drying lactose and mannitol aqueous solutions, Dry. Technol. (2018) 1–10, http://dx.doi.org/10.1080/07373937.2017.1399903.
[18] C. Song, J. Nam, A numerical study on freeze drying characteristics of cylindrical products with and without container, Int. J. Transport Phenom. 7 (3) (2005) 241.
[19] S.A. Velardi, A.A. Barresi, Development of simplified models for the freeze-drying process and investigation of the optimal operating conditions, Chem. Eng. Res. Des. 86 (1) (2008) 9–22.
[20] J. Welty, C. Wicks, R. Wilson, G. Rorrer, Fundamentals of Momentum, Heat, and Mass Transfer vol. 1, John Wiley and sons, Ltd, 2008.